Dipole Solvation: Nonlinear Effects, Density Reorganization, and the Breakdown of the Onsager Saturation Limit†

Anatoli Milischuk and Dmitry V. Matyushov*

Department of Chemistry and Biochemistry, Arizona State University, P.O. Box 871604, Tempe, Arizona 85287-1604

Received: July 3, 2001; In Final Form: October 31, 2001

Linear cavity solvation models predict saturation of the solvation chemical potential, $\mu_p \rightarrow$ *constant*, at high solvent polarity. This qualitative prediction is tested on computer simulations of dipole solvation in dipolar hard-sphere solvents in the liquid and solid phase states. We find that solvation saturation does exist for solid dipolar solvents, but does not exist for liquid dipolar solvents when the linear solvent response holds. Solvation saturation occurs due to nonlinear solvation in liquid solvents when solvent−solvent attractions exceed solute−solvent attractions. Nonlinear solvation is caused by electrostriction resulting in dewetting of the solute surface of a nonpolar or weakly polar dipolar solute. Solvation thermodynamics is affected by a combination of orientational and density solvent reorganization. The relative contribution of each component is strongly dependent on solvent polarity. In highly polar solvents, the orientational and density reorganization approximately equally contribute to the average solvation energy and the second solvation cumulant. The entropy of solvation is found to be positive and virtually independent of solvent polarity. This comes about as a result of a compensation between a negative solvation entropy due to orientational reorganization of the solvent and a positive solvation entropy due to density reorganization. The Onsager model does not provide even a qualitative account of solvation entropies. Our simulations give strong support to the Q-model of nonlinear solvation. Applications of the dipole solvation thermodynamics to electron-transfer reactions and optical spectroscopy are discussed.

1. Introduction

The Onsager model for solvation of a dipolar solute in a polar solvent[1] searches for a solution of the Poisson equation for a point dipole in a spherical cavity cut from a dielectric medium. The solute dipole moment, $\mathbf{m}_0$, interacts with the dielectric reaction field of the solvent, $\mathbf{R}$, resulting in the following solvation chemical potential

$$\mu_p = -\frac{1}{2}\mathbf{m}_0 \cdot \mathbf{R} \tag{1}$$

where "0" refers to the solute. The reaction field arises as a result of displacements in the solvent induced by the presence of the solute dipole. For spherical cavities considered in the Onsager model, it is fully defined by the solvent dielectric constant ϵ and the cavity radius a

$$\mathbf{R} = \frac{2(\epsilon - 1)}{2\epsilon + 1}\frac{\mathbf{m}_0}{a^3} \tag{2}$$

The Onsager approach sets up a closed, two-parameter model that does not assume any particular recipe for the calculation of either of its two parameters: the cavity radius a and the dielectric constant ϵ. The model has been widely used to treat solvent electrostatic effects on steady-state[2,3] and time-resolved[4] optical spectra, as well as other phenomena involving dynamics of polar interactions, dielectric friction[5] is an example. The Onsager model makes some important quantitative and qualitative predictions that are often adopted in the literature,[2−5] but still have not been thoroughly tested. From the qualitative side, the model gives a zero solvation chemical potential at $\epsilon \rightarrow 1$ and predicts a saturation limit

$$-\mu_p \rightarrow \frac{{m_0}^2}{2a^3} \tag{3}$$

at $\epsilon \rightarrow \infty$. The latter result is especially important for applications. Many liquid solvents commonly used in solution chemistry are polar liquids with $\epsilon \gg 1$. For such solvents, the model suggests very little sensitivity of μ_p to changes in solvent polarity and puts a significant emphasis on the way the cavity radius a is calculated. Indeed, numerous efforts have been undertaken to define the "best" effective radius for dipolar and ionic solutes.[6−12] However, the existence of the saturation limit itself has not been tested either on molecular solvation theories or computer simulations of solvation.

The qualitative test of the existence of the saturation limit in the linear response approximation (LRA), predicted by the Onsager model, is the aim of this study. We show that fast saturation of the solvation chemical potential with increasing solvent polarity, predicted by eqs 1 and 2, does not happen for model liquid solvents. Moreover, the LRA solvation chemical potential has a linear asymptote with increasing polarity of the solvent and we show how this linear trend can be exactly obtained in the linear solvation models (section 3). For liquid solvents, the outcome of solvation saturation turns out to be linked with nonlinear solvation. Computer simulations per-

† Part of the special issue "Noboru Mataga Festschrift".

* To whom correspondence should be addressed. E-mail: dmitrym@asu.edu. Fax: (480) 965-2747.

10.1021/jp012511t CCC: $22.00
Published on Web 00/00/0000 PAGE EST: 11.1

formed here show that dewetting of solute's surface in highly polar solvents is responsible for nonlinear solvation effects. Finally, in section 4, we discuss applications of solvation energetics considered here to electron-transfer reactions and optical spectroscopy.

2. Model

Testing the Onsager model is not straightforward as the macroscopic property, the dielectric constant, is employed to define the microscopic property, the solvation chemical potential. Molecular solvation models are commonly formulated in terms of microscopic solvent properties and do not always provide ϵ. That is why model condensed systems for which both the dielectric macroscopic properties and the microscopic solvation potential can be simultaneously calculated should be employed to establish the qualitative picture of the dependence of the solvation chemical potential on solvent polarity. Despite significant progress achieved in recent decades in understanding and describing molecular polar fluids, there are very few model systems for which sufficient molecular and macroscopic information is accumulated to provide a stringent test of dielectric models. One of such model system, that has played a significant role in developing our understanding of polar liquid thermodynamics[13,14] and physics of dielectric materials,[15] is the dipolar solvent, in the fluid[13−15] or solid[16] state. We consider here a dipolar hard sphere (HS) solvent composed of HSs of diameter σ bearing point dipoles m. The thermodynamic properties of the pure solvent are fully characterized by two dimensionless parameters: the reduced number density $\rho^* = \rho\sigma^3$ and the reduced dipolar density $y = (4\pi/9)\beta\rho m^2$. Here, ρ is the solvent number density and $\beta = 1/k_BT$; k_B is Boltzmann's constant and T is temperature.

Even for the most studied model of the HS dipolar fluid, the connection of the microscopic parameter y to the macroscopic dielectric constant is not easy to establish. The Kirkwood equation

$$\frac{(\epsilon - 1)(2\epsilon + 1)}{9\epsilon} = g_K(y)y \tag{4}$$

contains a generally unknown dependence of the Kirkwood factor g_K on y. The Kirkwood factor can be calculated from integral equation theories[13] or perturbation expansions.[17] Both approaches, however, fail at large y.[18] Therefore, an empirical equation for $\epsilon(y)$ reproducing computer simulation results has been recently proposed[18]

$$\epsilon(y) - 1 = 3y + 3y^2 + (2/p^2)[\exp(3p^3y^3/2) - 1] \tag{5}$$

Equation 5 makes use of the perturbation expansion theory for the dielectric constant by Tani et al[17] with the parameter $p = 9I_{dd\Delta}(\rho^*)/16\pi^2 - 1$ defined through a three-particle perturbation integral $I_{dd\Delta}(\rho^*)$ depending on the reduced density ρ^*.[17] Equation 5 was shown to agree with simulated dielectric constants of pure HS dipolar fluids in the range $1 \le \epsilon \le 220$. The connection between ϵ and y opens a door to the comparison of the dielectric cavity models, operating in terms of dielectric constants, to molecular descriptions of solvation, operating in terms of the parameter y, in a broad range of solvent polarities.

A comparison of the molecular solvation models to the dielectric cavity description demands definition of the cavity radius a, which is not specified within cavity models. For our qualitative analysis of the Onsager picture, it suffices to say that the model consistency implies that the radius a is independent of the solvent dielectric constant and, consequently, of solvent polarity. To be specific, we will consider a HS solute of the radius R_0 and will assume $a = R_0$ throughout the paper.

Solvation of a HS dipolar solute in a HS dipolar solvent is fully characterized by two solvent parameters, ρ^* and y, and by two solute parameters, R_0 and m_0. The latter two can be combined in one dimensionless parameter characterizing the dipolar strength of the solute

$$(m_0^*)^2 = \beta {m_0}^2/{\sigma_0}^3, \quad \sigma_0 = 2R_0 \tag{6}$$

This parameter is defined analogously to the effective dipolar strength of the pure solvent, $(m^*)^2 = \beta m^2/\sigma^3$ ($y = (4\pi/9)\rho^*(m^*)^2$).[13]

3. Solvation Thermodynamics

3.1. Linear Response Approximation. The Onsager model assumes linear solvent response. This implies that the reaction field is a linear function of the solute dipole moment (eq 2) and the solvation chemical potential is quadratic in m_0 (eq 1). This assumption leads to several general relations which can be directly tested on computer simulations. First, the solvation chemical potential μ_p is one-half of the average solute−solvent interaction energy $\langle u_{0s}\rangle$

$$\mu_p = \frac{1}{2}\langle u_{0s}\rangle \tag{7}$$

Here, u_{0s} is the solute−solvent interaction potential ("s" stands to the solvent) and $\langle ...\rangle$ refers to the statistical average over the solvent configurations in equilibrium with the solute. Further, the first and second cumulants of the solute−solvent interaction potential are connected to each other as follows[18]

$$-\langle u_{0s}\rangle = \beta\langle(\delta u_{0s})^2\rangle \tag{8}$$

Finally, when the second cumulant is calculated in the LRA, the distribution of the solvent molecules around the solute is not perturbed by the solute−solvent dipole−dipole interaction. The solute−solvent distribution used to calculate $\langle(\delta u_{0s})^2\rangle$ then remains the same for all magnitudes of m_0. For a stringent test of this requirement, one can consider the condition

$$\langle(\delta u_{0s})^2\rangle = \langle(\delta u_{0s})^2\rangle_0 \tag{9}$$

where $\langle ...\rangle_0$ refers to the statistical average over the solvent configurations in equilibrium with the solute with zero dipole moment.

Molecular solvation models do not support the existence of a saturation limit $\mu_p \rightarrow$ *constant* for the solvation chemical potential within the LRA. The mean-spherical approximation (MSA) for dipole solvation[19] leads to a linear dependence

$$-\mu_p^{MSA} \propto y \tag{10}$$

at large y. The MSA solution is an approximation. However, the linear trend $-\mu_p \propto y$ can be proved exactly, based on some very general properties of dipolar fluids. For this one can use the connection between the solvation chemical potential and the second cumulant of the solute−solvent interaction potential (eqs 7 and 9), $-\mu_p = (\beta/2)\langle(\delta u_{0s})^2\rangle_0$. The latter can be written explicitly[20] to give the solvation chemical potential in the form

$$-\beta\mu_p/{m_0}^2 = yR_{eff}^{-3}(\rho^*,r_{0s}) + y[2q_L(\rho^*,r_{0s},y) + q_T(\rho^*,r_{0s},y)] \tag{11}$$

In eq 11,

$$R_{\mathrm{eff}}^{-3}(\rho^*,r_{0s}) = 3\int_0^\infty (\mathrm{d}r/r^4) g_{0s}^{(0)}(r,\rho^*,r_{0s}) \qquad (12)$$

is the effective radius of a HS solute in a HS solvent.[18] It includes local packing effects of the repulsive hard cores of the solvent molecules around the solute and, therefore, depends on the solvent reduced density ρ^* and the solute/solvent size ratio $r_{0s} = R_{0s}/\sigma$, $R_{0s} = R_0 + \sigma/2$ through the solute−solvent HS distribution function $g_{0s}^{(0)}(r,\rho^*,r_{0s})$. The latter describes packing of HS molecules around a HS solute and is not affected by any long-range interactions; for brevity, we will suppress the dependence on ρ^* and r_{0s} in $g_{0s}^{(0)}(r,\rho^*,r_{0s})$ in the remainder.

The first summand in eq 11 is the one-particle solvent response which is simply proportional to the density of dipoles in the liquid. The second term arises from many-particle solvent−solvent interactions which screen the distortions induced by the solute. The first summand is positive and the second summand is negative, thus reducing the direct one-particle response. The polarity dependence of the many-particle solvent response entering the functions

$$q_{\mathrm{L,T}}(\rho^*,r_{0s},y) = \frac{1}{\pi}\int_{-\infty}^{\infty} (f^{(2)}(k))^2 [S_{\mathrm{L,T}}(k) - 1] k^2 \, \mathrm{d}k \qquad (13)$$

is determined by, correspondingly, the longitudinal, $S_{\mathrm{L}}(k)$, and transverse, $S_{\mathrm{T}}(k)$, structure factors of the solvent polarization. The structure factors $S_{\mathrm{L,T}}(k)$ are defined through the corresponding correlators of the longitudinal and transverse polarization fluctuations of the polar liquid[21]

$$\langle |\delta P_{\mathrm{L}}(k)|^2 \rangle = (Nm^2/3) S_{\mathrm{L}}(k)$$

$$\langle |\delta P_{\mathrm{T}}(k)|^2 \rangle = (2Nm^2/3) S_{\mathrm{T}}(k) \qquad (14)$$

where $\delta P_{\mathrm{L}}(k)$ and $\delta P_{\mathrm{T}}(k)$ stand for the Fourier transforms of the longitudinal and transverse polarization fluctuations of the pure solvent; N is the number of solvent molecules. In eq 13,

$$f^{(2)}(k) = \int_0^\infty \frac{\mathrm{d}r}{r} g_{0s}^{(0)}(r) j_2(kr) \qquad (15)$$

where $j_2(x)$ is the second-order spherical Bessel function.[22]

In the limit of large y, the longitudinal structure factor vanishes in the range of k values contributing significantly to the integral in eq 13. The transverse structure factor, on the contrary, peaks strongly at $k = 0$ (Figure 1). At large y, the transverse structure factor is very well reproduced by the $k \to 0$ expansion of the corresponding direct correlation function $c_{\mathrm{T}}(k)$ truncated at the second in k expansion term. This leads to the Ornstein−Zernike approximation[23] for the transverse structure factor

$$S_{\mathrm{T}}(k) = \frac{S_{\mathrm{T}}(0) + k^2 \Lambda_{\mathrm{T}}^2}{1 + k^2 \Lambda_{\mathrm{T}}^2} \qquad (16)$$

where at $k = 0$[24]

$$S_{\mathrm{T}}(0) = (\epsilon - 1)/3y \qquad (17)$$

The correlation length Λ_{T} determines the exponential long-distance decay of the transverse polarization fluctuations

$$\langle \delta P_{\mathrm{T}}(r) \delta P_{\mathrm{T}}(0) \rangle \propto r^{-1} \mathrm{e}^{-r/\Lambda_{\mathrm{T}}} \qquad \text{at} \qquad r \to \infty \qquad (18)$$

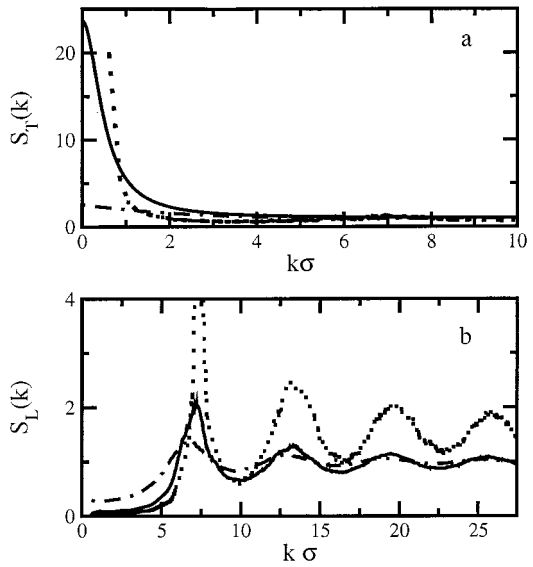

Figure 1. Transverse (a) and longitudinal (b) structure factors of HS dipolar solvents at $(m^*)^2 = 1.0$ (dash−dotted line), $(m^*)^2 = 4.0$ (solid line), and $(m^*)^2 = 7.0$ (dotted line). Plotted are simulation results with 864 solvent molecules in a cubic simulation box; the simulation length is 6.5×10^5 cycles.

These two general properties of the longitudinal and transverse structure factors in the limit of large y values lead directly to the exact asymptote at $y \to \infty$ in eq 11

$$-\beta\mu_{\mathrm{p}}/ym_0^2 = R_{\mathrm{eff}}^{-3} - 2\int_0^\infty (\mathrm{d}r_1/r_1^4) g_{0s}^{(0)}(r_1)[g_{0s}^{(0)}(r_1) - (\kappa_{\mathrm{T}}/5\sigma^2)\int_0^{r_1} r_2 g_{0s}^{(0)}(r_2)\, \mathrm{d}r_2] \qquad (19)$$

The result is an obviously linear dependence of μ_{p} on y with the slope depending on the solvent reduced density ρ^*, the solute−solvent size ratio R_0/σ, and the parameter

$$\kappa_{\mathrm{T}} = \lim_{y\to\infty} \frac{S_{\mathrm{T}}(0)\sigma^2}{\Lambda_{\mathrm{T}}^2} \qquad (20)$$

In the MSA,[25] $S_{\mathrm{T}}(0) \to \infty$ and $\Lambda_{\mathrm{T}} \to \infty$ at $y \to \infty$, but the parameter κ_{T} tends to a constant limit, $\kappa_{\mathrm{T}} = 3$. The exact value of this parameter for dipolar solvents is unknown.

The derivation presented here strongly suggests that the existence of the Onsager saturation limit and the LRA cannot be reconciled with each other. In contrast to the Onsager model giving $\mu_{\mathrm{p}} \to$ *constant*, molecular solvation theories predicts $\mu_{\mathrm{p}} \propto y$ at large y as long as the LRA holds. Going beyond the LRA within analytical solvation models inevitably involves approximations[26] and we thus need to turn to computer simulations to obtain the "exact" dependence of thermodynamic solvation parameters on y for solvation in the model solvent of HS dipoles.

3.2. Computer Simulations. Computer Monte Carlo (MC) simulations of a HS dipole solute in a HS dipolar solvent were carried out as described elsewhere.[18] All simulations were performed for $r_{0s} = 1.4$ and $\rho^* = 0.8$. A cubic cell with a single solute and 500 solvent molecules was employed to simulate the first and second cumulants of the solute−solvent interaction energy (Table 1). The simulation cell with 864 solvent molecules was used to obtain the longitudinal and transverse structure factors of the pure dipolar solvent (Figure 1). The simulations were set up to provide a comprehensive test of both the LRA and the existence of the polarity saturation limit within the LRA

TABLE 1: Simulated Solvation Cumulants and Calculated Chemical Potentials of Solvation in Liquid Dipolar HS Solvents

	$m_0/m = 4.0$		$m_0 = 0 (m_0^*)^2 = 2.74$					$m_0 = 0$
$(m^*)^2$	$-\langle u_{0s}\rangle^a$	$\langle(\delta u_{0s})^2\rangle^b$	$-\langle u_{0s}\rangle^a$	$\langle(\delta u_{0s})^2\rangle^b$	$-2\mu_p{}^c$	$-2\mu_p{}^d$	γ	$\langle(\delta u_{0s})^2\rangle_0{}^e$
0.5	2.43	2.40	2.44	2.30	2.42	2.41	0.9988	2.42
1.0	3.43	3.40	3.44	3.26	3.41	3.39	0.9990	3.43
1.5	4.03	4.06	3.98	3.97	3.98	3.98	1.0000	3.97
2.0	4.38	4.17	4.38	4.32	4.34	4.32	1.0004	4.35
2.5	4.57	4.57	4.62	4.57	4.63	4.63	1.0002	4.53
3.0	4.78	4.53	4.75	4.78	4.76	4.77	1.0000	4.71
3.5	4.87	4.87	4.87	4.90	4.91	4.93	1.0005	4.68
4.0	5.09	5.09	4.93	5.08	5.00	5.01	1.0001	4.75
4.5	5.20	5.44	5.08	5.19	5.15	5.19	1.0014	4.74
5.0	5.35	5.49	5.10	5.34	5.17	5.21	0.9997	4.91
5.5	5.41	5.39	5.18	5.58	5.30	5.36	0.9996	4.83
6.0	5.53	5.61	5.18	5.63	5.32	5.40	1.0001	4.75
6.5	5.64	5.59	5.18	5.77	5.34	5.42	0.9977	4.82
7.0	5.66	5.58	5.10	5.90	5.26	5.32	0.9930	4.78
7.5	5.76	5.85	5.05	5.85	5.27	5.38	0.9973	4.48
8.0	5.79	6.06	5.04	6.21	5.38	5.53	0.9961	4.19
8.5	5.82	5.82	4.99	6.62	5.38	5.50	0.9828	4.41

[a] $-\beta\langle u_{0s}\rangle/(m_0^*)^2$. [b] $\beta^2\langle(\delta u_{0s})^2\rangle/(m_0^*)^2$. [c] $-2\beta\mu_p/(m_0^*)^2$ according to eq 34. [d] $-2\beta\mu_p/(m_0^*)^2$ according to eq 36. [e] The second solvation cumulant is obtained by adopting a nonzero solute dipole in the solute−solvent interaction potential and calculating the average over the solvent configurations in equilibrium with a nonpolar solute ($m_0 = 0$). The listed data refer to the reduced cumulants, $\beta^2\langle(\delta u_{0s})^2\rangle_0/(m_0^*)^2$, that are independent of the choice of the solute dipole.

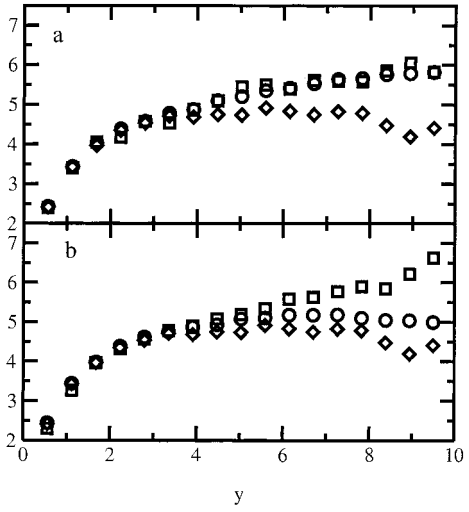

Figure 2. $-\beta\langle u_{0s}\rangle/(m_0^*)^2$ (squares), $\beta^2\langle(\delta u_{0s})^2\rangle/(m_0^*)^2$ (circles), and $\beta^2\langle(\delta u_{0s})^2\rangle_0/(m_0^*)^2$ (diamonds) vs y at $m_0/m = 4.0$ (a) and $(m_0^*)^2 = 2.74$ (b).

predicted by the Onsager model (eq 3). Three configurations for the solute were considered. In the first set of simulation runs, the solute−solvent dipole moment ratio was kept constant ($m_0/m = 4.0$) and the solvent reduced dipole moment $(m^*)^2$ was varied in the range 0.5−8.5. In the second set of data, the solute dipole moment was fixed at $(m_0^*)^2 = 2.74$ and $(m^*)^2$ was varied. Finally, the third set of simulations was obtained by varying $(m^*)^2$ at $m_0 = 0$. The first and second cumulants of the solute−solvent interaction ($\langle u_{0s}\rangle_0 = 0$) are listed in Table 1.

Figure 2 shows that the LRA actually breaks down for polar solvents with $y > 5$. Equation 8 approximately holds for the simulations with constant solute/solvent dipole ratio $m_0/m = 4.0$. However, eq 9 becomes inaccurate up to 35%. The polarity dependence of the second cumulant $\langle(\delta u_{0s})^2\rangle_0$ is especially indicative of nonlinear solvation. Instead of a linear trend $\propto y$

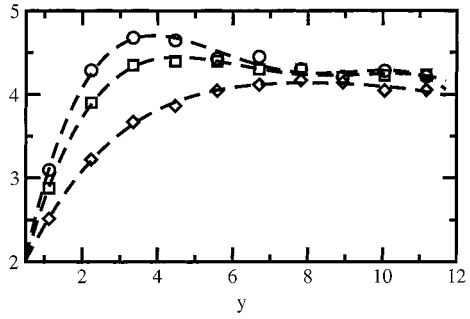

Figure 3. $-\beta\langle u_{0s}\rangle/(m_0^*)^2$ (squares), $\beta^2\langle(\delta u_{0s})^2\rangle/(m_0^*)^2$ (circles), and $\beta^2\langle(\delta u_{0s})^2\rangle_0/(m_0^*)^2$ (diamonds) vs y in fcc crystalline solvents; $(m_0^*)^2 = 2.74$. Dashed lines are regressions through the points.

predicted by linear response molecular models, the second cumulant goes through a broad maximum starting to decay with increasing y. When the solute dipole is kept constant while increasing the solvent polarity, the solvation energy does show a saturation limit, but the second cumulant $\langle(\delta u_{0s})^2\rangle$ increases approximately linearly with y (Figure 2b).[27] The saturation limit is thus a result of purely nonlinear solvation effects (see below).

The deviation between the first, $-\langle u_{0s}\rangle$, and the second, $\beta\langle(\delta u_{0s})^2\rangle$ and $\beta\langle(\delta u_{0s})^2\rangle_0$, cumulants seen for solvation in HS liquid solvents is not observed if a lattice of point dipoles is used as a solvent. Figure 3 shows the dependence of the first and two second cumulants of the solute−solvent interaction potential on y at constant m_0. Despite considerable deviations between $\langle u_{0s}\rangle$, $\langle(\delta u_{0s})^2\rangle_0$, and $\langle(\delta u_{0s})^2\rangle$ at medium polarities, they all tend to the same saturation limit at large y values. Interestingly, the LRA holds for dipolar solvation in highly polar dipolar lattices. The qualitative distinction between the polarity dependence of the second cumulants obtained for dipolar liquids and dipolar solids suggests that it may be caused by local density changes that are allowed in a liquid solvent, but are suppressed in a lattice solvent.

3.3. Dielectric Saturation and Electrostriction. Nonlinear solvation in polar solvents is commonly related to a combined effect of dielectric saturation and electrostriction. Dielectric saturation refers to orientational ordering of the solvent molecules in an external electric field.[15] If the solvent dipoles are oriented so that no further orientation is possible, the dielectric solvent response is lower than that expected from the LRA. Dielectric saturation is accounted for by allowing the dielectric constant to change with distance from the solute[6−8] or by adopting the Langevin formula for dipoles' orientations.[16] Electrostriction stands for local density changes in solute's vicinity produced by its electric field.[15] The latter effect is often described in terms of the *solute* cavity radius depending on the strength of the electric field[9] or an effective *solvent* radius for the first solvation shell molecules.[10] Electrostriction is commonly expected to bring solvent molecules into closer contact with the solute, hence increasing the solvation power of the solvent.[28] The mutual compensation of dielectric saturation and electrostriction is believed to be responsible for the remarkable accuracy of the LRA in dense liquid solvents, despite strong electric fields existing on molecular lengthscales.[29] The simulation results provided in this study for a range of dipolar solvents existing in both the solid and liquid states allow us to separate the relative contributions of dielectric saturation and electrostriction to solvation thermodynamics.

To quantify electrostriction and dielectric saturation we will consider two radial distributions

$$N_0(r) = 4\pi\rho r^2 g_{0s}(r) \tag{21}$$

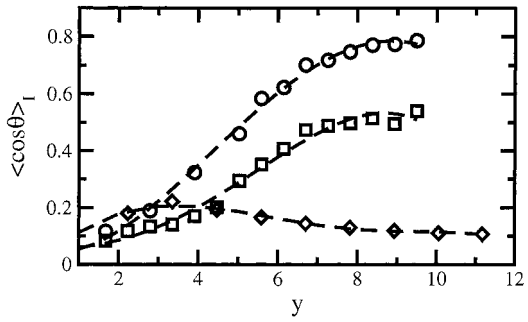

Figure 4. Average cosine of the angle between the solute and solvent dipoles for the solvent molecules in the first solvation shell (eq 25) measured for fcc-lattices (diamonds) and for dipolar liquid solvents at $(m_0^*)^2 = 2.74$ (squares) and $m_0/m = 4.0$ (circles). The dashed lines are drawn to guide the eye.

and

$$N_1(r) = (4\pi/3)\rho r^2 h_{0s}^{110}(r) \tag{22}$$

The first one, $N_0(r)$, gives the radial distribution of the number of solvent molecules around the solute; $g_{0s}(r)$ is the radial distribution function. The second, $N_1(r)$, gives the radial distribution of the average cosine of the angle between the solvent and solute dipole moments. In eq 22, $h_{0s}^{110}(r)$ is a rotation invariant projection[13] of the orientation-dependent solute−solvent correlation function $h_{0s}(01)$

$$h_{0s}^{110}(r) = 3\int h_{0s}(01)(\hat{\mathbf{s}}_0 \cdot \hat{\mathbf{s}})\, d\Omega_0\, d\Omega/(4\pi)^2 \tag{23}$$

where $\hat{\mathbf{s}}_0 = \mathbf{m}_0/m_0$ and $\mathbf{s} = \mathbf{m}/m$; 0 and 1 stand for the coordinates and orientations of the solute and a solvent molecule, respectively. Nonlinear effects are largely local,[9,29] and we will consider the number of solvent molecules in the first solvation shell

$$N_I = \int_{R_0+\sigma/2}^{R_0+\sigma} N_0(r)\, dr \tag{24}$$

and the average cosine in the first solvation shell

$$\langle \cos\theta \rangle_I = \int_{R_0+\sigma/2}^{R_0+\sigma} N_1(r)\, dr/N_I \tag{25}$$

where $\cos\theta = \hat{\mathbf{s}}_0 \cdot \hat{\mathbf{s}}$.

Judged from the ratio $\beta\langle(\delta u_{0s})^2\rangle/\langle u_{0s}\rangle$ in Figure 3 and the average cosine of the solvent molecules in the first solvation shell (eq 25, Figure 4, diamonds), the nonlinear effect due to saturation of dipoles' orientations in a lattice solvent passes through a maximum at $(m^*)^2 \simeq 3$. This magnitude of the solvent effective dipole is in fact close to the effective solute dipole $(m_0^*)^2 = 2.74$. The nonlinear dielectric saturation thus maximizes at a resonance of the strengths of solute−solvent and solvent−solvent interactions. A similar effect was observed previously by Åqvist and Hansson for dipolar solutes in water.[30,31] The maximum of nonlinear solvation was attributed to the collapse of the H-bond network at the resonance of the solute−solvent and solvent−solvent interactions. The fact that we observe here exactly the same behavior for dipolar solvents suggests that a maximum in dielectric saturation is a general phenomenon related to the competition between solute−solvent and solvent−solvent attraction forces. Increasing the solvent polarity from zero to $m^* \simeq m_0^*$ enhances the electric field acting on solvent dipoles, thus leading to dielectric saturation. At $m^* > m_0^*$, the solvent−solvent attractions gain importance

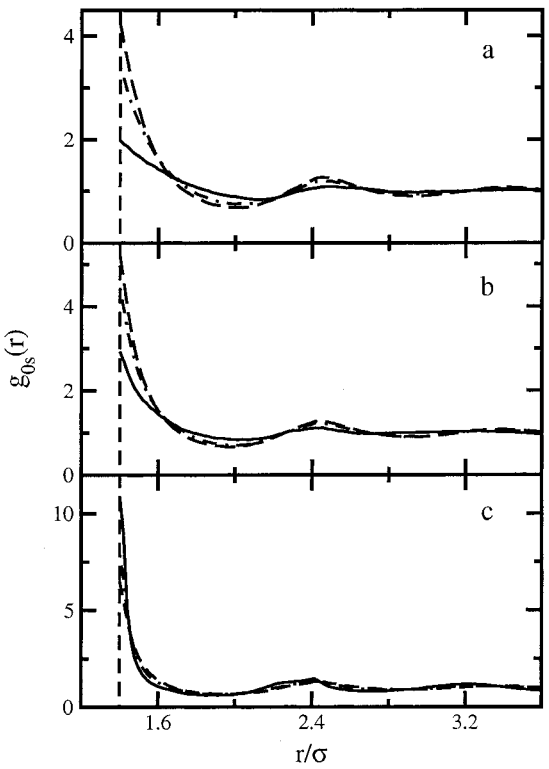

Figure 5. Solute-solvent radial pair distribution function for $m_0 = 0$ (a), $(m_0^*)^2 = 2.74$ (b), and $m_0/m = 4.0$ (c). Solvent polarities are $(m^*)^2 = 2.5$ (dashed lines), $(m^*)^2 = 4.5$ (dot−dashed lines), and $(m^*)^2 = 8.5$ (solid lines). The vertical dashed lines indicate the distance of the closest approach, $r/\sigma = r_{0s}$, of the solute and solvent HSs.

and orientations of the solvent molecules become closer to those in a pure polar liquid. The dielectric saturation then decays and the solvent response gets closer to the LRA prediction (Figure 3). No such effect is, however, observed in dipolar liquid solvents (squares and circles in Figure 4). The average cosine shows a behavior reminiscent of that in the Langevin model[16] changing from zero to some saturation limit determined by the magnitude of the solute dipole. This dependence is not, however, solely an orientational response, but a combined effect of changes in average angles and coordinates of the first-shell solvent molecules.

A qualitative understanding of the effect of electrostriction on solvation can be gained from looking at $g_{0s}(r)$ at various y values. The most significant effect of increasing solvent polarity on $g_{0s}(r)$ is seen for the nonpolar HS solute, $m_0 = 0$ (Figure 5a). The contact values $g_{0s}(R_{0s})$ decrease considerably with increasing y (diamonds in Figure 6a), the peak of the second solvation shell shifts away from the solute (Figure 5a), and, generally, $g_{0s}(r)$ becomes increasingly shallow in more polar solvents. The number of solvent molecules in the first solvation shell (Figure 6b) follows the trend in $g_{0s}(R_{0s})$ producing a substantial dewetting of the solute surface in strongly polar solvents. This local softening of the solvent structure, analogous to Stillinger's dewetting of hydrophobic surfaces,[32,33] was obtained also for dipolar liquids in contact with neutral planar surfaces.[34] For nonpolar solutes, dipolar solvent−solvent attractions are not compensated by solute−solvent interactions leading to lower local density around the solute. Similar, but less pronounced, effect is seen when the solute has a constant dipole moment (Figure 5b, squares in Figure 6). On the other hand, for the set of simulations with the constant ratio $m_0/m = 4.0$ (Figure 5c, circles in Figure 6), the reduced solute, m_0^*, and solvent, m^*, dipole moments are close to each other ($m_0^*/m^* =$

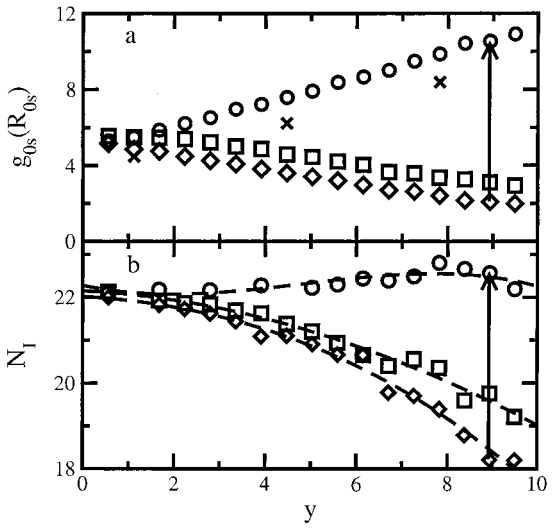

Figure 6. Contact value of the solute−solvent radial distribution function $g_{0s}(R_{0s})$ (a) and the number of solvent molecules in the first solvation shell (eq 24, b) vs y for $m_0 = 0$ (diamonds), $(m_0^*)^2 = 2.74$ (squares), and $m_0/m = 4.0$ (circles). Crosses (a) indicate contact values for the solvent−solvent radial distribution function, $g_{ss}^{000}(\sigma)$. The arrows show a vertical transition with the dipole change $0 \rightarrow m_0$ (see the text).

1.66) and no dramatic changes in the local density occur (Figure 6b), despite the fact that the contact value $g_{0s}(R_{0s})$ grows with solvent polarity (Figures 5c and 6a, circles). In this latter case, the radial distribution function does not significantly change outside a very narrow contact region and the growth of the contact value does not strongly affect the population of the first solvation shell. The increase in $g_{0s}(R_{0s})$ goes in parallel with a concomitant increase in the solvent−solvent contact value $g_{ss}^{000}(\sigma)$ (crosses in Figure 6a). The structure of the solvent in the solute vicinity is then not much different from the bulk and the solvent molecules on the solute surface and in the bulk respond in a similar fashion. The result is essentially a linear solvent response, $-\langle u_{0s}\rangle \simeq \beta\langle(\delta u_{0s})^2\rangle$, to the solute electric field.

Contact values of the solvent−solvent pair distribution function obtained here from simulations allow us to test the RHNC approximation developed to take into account the nonlinear aspects of solvation on the level of the hypernetted-chain closure relation.[26] For the first three angular projections of the solvent−solvent pair distribution function appearing in linear theories of dipolar fluids,[25] $\{g_{ss}^{000}(\sigma), h_{ss}^{110}(\sigma), h_{ss}^{112}(\sigma)\}$, our simulations yield {4.92, 3.65, 4.66} and {5.27, 5.03, 5.73} at $(m^*)^2 = 2.0$ and 2.75, respectively. These data are to be compared with the RHNC result: {4.57, 2.90, 4.13} and {4.92, 4.24, 5.21}. The effect of dipolar interactions on the density and angular distribution of the solvent molecules is therefore systematically underestimated on the RHNC level of the theory even for relatively small solvent polarities.

The analysis of relative effects of electrostriction and dielectric saturation allows us to draw some conclusions regarding the origin of nonliner dipolar solvation in dipolar liquid solvents. Dielectric saturation reaches its maximum at intermediate polarities $m^* \simeq m_0^*$ (Figures 3 and 4). In this polarity range, dielectric saturation is fully compensated by electrostriction of the first solvation shell. As a result, eqs 8 and 9 are fulfilled and the system shows the linear solvent response. The nonlinear separation of the first and second solvation cumulants occurs at higher solvent polarities. It is chiefly caused by a substantial dewetting of the solute surface for nonpolar solutes for which the strongest nonlinear effect is

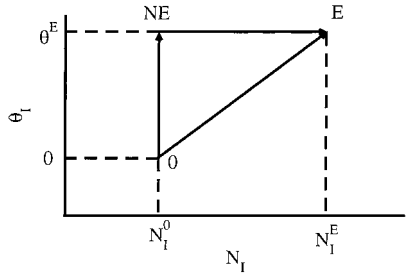

Figure 7. Transition from the nonpolar, $m_0 = 0$, state (0) to an equilibrium state (E) with $m_0/m = 4.0$ in the coordinates of the first solvation shell population, N_I, and the average angle of the solvent dipoles relative to the solute dipole, θ_I. "NE" denotes the nonequilibrium state at which the orientational stress is relaxed, but the coordinates of the solvent molecules are in equilibrium with the nonpolar state.

observed ($\langle(\delta u_{0s})^2\rangle_0$ in Figure 2). On the opposite side, a relatively weak modulation of N_I at $m_0/m = constant$ gives rise to a nearly perfect equality between $\beta\langle(\delta u_{0s})^2\rangle$ and $-\langle u_{0s}\rangle$ and a linear solvent response. According to the LRA, a linear trend $\propto y$ is then seen for the solvation chemical potential.[27]

3.4. Orientational and Density Reorganization. The inspection of Figures 5 and 6 shows that a vertical, optical excitation of a solute changing its dipole moment creates a strain in the solvent in respect to both orientations and positions of the solvent molecules. The transition shown by the vertical lines in Figure 6 corresponds to a dipole change $0 \rightarrow 15$ D within a solute of the radius $R_0 = 3.7$ Å in a solvent with the dipole moment 4.8 D if one assumes $\sigma = 4.141$ Å characteristic of acetonitrile.[35] [Both solute and solvent dipoles may refer to their polarizability-renormalized values (see Discussion).] This vertical transition creates a nuclear strain corresponding to the change in the average first solvation shell cosine from 0 to 0.77 (Figure 4) and the average number of solvent molecules in the first solvation shell from 18.2 to 22.6 (Figure 6). Relaxation of the nuclear subsystem into equilibrium with the new charge distribution hence involves reorientation of the solvent molecules (orientational reorganization) and a change in the local density around the solute (density reorganization). The separation of the solvent reorganization into orientational and density components is important for both the dynamics and thermodynamics of the solvent response. Solvent translations significantly alter the solvation time correlation function.[36] For the static response, the density component of solvent reorganization is the main contribution to the solvation entropy due to its stronger temperature dependence (see below).[37]

To separate the overall solvent response into the orientational and density components, we follow the procedure suggested by time-resolved Stokes shift experiments.[38] Full equilibration after a sudden transition from $m_0 = 0$ to $m_0 > 0$ involves the relaxation of both the orientational and density strains. This full equilibration, corresponding to the total Stokes shift in a time-resolved experiment, is shown by the arrow $0 \rightarrow$ E in Figure 7. This equilibrium state can be achieved in two steps: first relaxing the orientational strain along the line $0 \rightarrow$ NE to a nonequilibrium state NE and then relaxing the density strain along the line NE $\rightarrow$ E.

We applied this two-step procedure in our MC simulations. Equilibrium system configurations corresponding to $m_0 = 0$ were taken with the intervals of $(3-4) \times 10^4$ MC cycles over all molecules in the simulation box as starting points of simulations of the same length in which $m_0/m = 4.0$ was adopted and only molecular orientations were equilibrated. The total equilibrium configuration file at $m_0 = 0$ of the length $(1.1-1.4) \times 10^6$ cycles was used to average the results of each such

TABLE 2: Orientational and Density Components of the First and Second Solvation Cumulants at $m_0/m = 4.0$

$(m^*)^2$	$-\beta\langle u_{0s}\rangle_{NE}^{or}$	$-\beta\langle u_{0s}\rangle_{NE}^{dens}$	$\beta^2\langle(\delta u_{0s})^2\rangle_{NE}^{or}$	$(\sigma_{NE}^{or})^a$	$\beta^2\langle(\delta u_{0s})^2\rangle_{NE}^{dens}$	$\beta^2\langle(\delta u_{0s})^2\rangle_{E}^{or}$	$(\sigma_{E}^{or})^b$	$\beta^2\langle(\delta u_{0s})^2\rangle_{E}^{dens}$
1.0	9.13	0.28	8.63	0.60	0.69	8.94	0.56	0.38
2.0	22.28	1.78	20.20	1.42	2.70	22.01	1.60	0.89
3.0	37.40	1.90	33.00	2.97	4.30	33.95	2.60	3.35
4.0	48.10	7.80	42.50	4.18	13.41	45.07	4.82	10.84
5.0	55.93	17.50	47.90	5.35	27.46	52.10	6.12	23.26
6.0	63.49	27.51	55.97	6.06	36.38	54.63	5.12	37.72
7.0	68.60	40.10	60.00	8.50	47.25	59.77	5.98	47.48
8.0	72.60	54.80	64.30	12.00	68.70	65.50	7.96	67.50

[a] Variance of the distribution of second cumulants $\beta^2\langle(\delta u_{0s})^2\rangle$ measured on different trajectories generated by the dipole switch $0 \rightarrow m_0$. [b] Variance of the distribution of second cumulants $\beta^2\langle(\delta u_{0s})^2\rangle$ generated by freezing molecular translations in solvent configurations in equilibrium with the solute.

trajectory over the initial equilibrium configurations. In this way, the orientational and density components of the first two solvation cumulants were generated (Table 2)

$$\langle u_{0s}\rangle = \langle u_{0s}\rangle_{NE}^{or} + \langle u_{0s}\rangle_{NE}^{dens}$$

$$\langle(\delta u_{0s})^2\rangle = \langle(\delta u_{0s})^2\rangle_{NE}^{or} + \langle(\delta u_{0s})^2\rangle_{NE}^{dens} \qquad (26)$$

The splitting in eq 26 assumes that orientational and density relaxations are uncoupled. The two modes are uncoupled indeed for symmetry reasons in the linear response,[25,37] but can couple to each other in the nonlinear response.[26] For two uncoupled Gaussian solvent modes linearly coupled to the solute, the second cumulant of the solute−solvent potential calculated for one of them is independent of another one. If that were the case, the second cumulant $\langle(\delta u_{0s})^2\rangle_{NE}^{or}$ calculated by relaxing the orientational strain after a solute dipole switch would be independent of the equilibrium configuration from which the simulation has been started. In fact, there is a variation in $\langle(\delta u_{0s})^2\rangle_{NE}^{or}$ measured on different trajectories and the variance of $\langle(\delta u_{0s})^2\rangle_{NE}^{or}$ given in Table 2 (σ_{NE}^{or}) gives an estimate of the orientational-density coupling. This latter does not exceed 20% of $\langle(\delta u_{0s})^2\rangle_{NE}^{or}$, which is roughly equal to the nonlinear solvation effect estimated from the comparison of $\langle(\delta u_{0s})^2\rangle$ and $\langle(\delta u_{0s})^2\rangle_0$ at $m_0/m = 4.0$ (Table 1).

To test the consistency of our results obtained by the sudden switch of the solute dipole with the linear response observed for $m_0/m = 4.0$, we carried out additional simulations in which we suppressed translations in the final equilibrium configuration (E) and measured only the fluctuation of the solute−solvent potential produced by orientational fluctuations. The average $\langle(\delta u_{0s})^2\rangle^{or}$ obtained on different trajectories over the initial configurations belonging to the equilibrium state E yields the orientational component of the second solvation cumulant, $\langle(\delta u_{0s})^2\rangle_{E}^{or}$. The corresponding splitting of the second cumulant is then

$$\langle(\delta u_{0s})^2\rangle = \langle(\delta u_{0s})^2\rangle_{E}^{or} + \langle(\delta u_{0s})^2\rangle_{E}^{dens} \qquad (27)$$

As is seen in Table 2, the second cumulants $\langle(\delta u_{0s})^2\rangle_{NE}^{or}$ and $\langle(\delta u_{0s})^2\rangle_{E}^{or}$ are really close to each other, as it should be expected for a linear solvent response. Furthermore, there is a fairly good agreement between the splitting of the average energy and the splitting of the second cumulants into the orientational and density components (Table 2).

The most interesting result of these simulations is a substantial dependence of the fraction of density reorganization in the solvent response on solvent polarity. The density component in both $\langle u_{0s}\rangle$ and $\langle(\delta u_{0s})^2\rangle$ is almost vanishing at $y \leq 3$, but rises quickly with increasing y matching the orientational component of the response in strongly polar solvents (Figure 8). A considerable component of density reorganization in the solvent response observed here for strongly polar solvents may seem to disagree with the results of the instantaneous normal mode (INM) analysis[39a] predicting a predominantly rotational (orientational) nature of the solvent response.[39b] More recent calculations by Ladanyi and Maroncelli (LM),[40a] using Steele's decoupling of rotations and translations in time-correlation functions,[40b] showed about 20% of the translational component to the frequency ω_s of the short-time, Gaussian part of the time-correlation function ($\propto\exp(-\omega_s^2t^2/2)$) of a dipolar solute. Our results, however, cannot be compared to LM calculations and INM models, as all of them refer to the early outcome of solvation dynamics, whereas our calculations refer to the static $t \rightarrow \infty$ limit of the solvent response. This static response has more bearing on the results of Bagchi and co-workers on the long-time, translational diffusion effects on solvation dynamics.[36] A more detailed analysis of the orientational-density splitting in the static solvent response will be presented elsewhere.

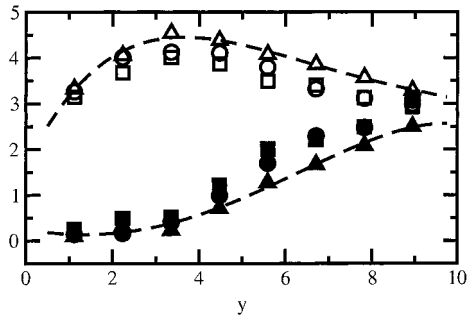

Figure 8. Orientational (open points) and density (filled points) components of $-\beta\langle u_{0s}\rangle/(m_0^*)^2$ (triangles) and $\beta^2\langle(\delta u_{0s})^2\rangle/(m_0^*)^2$ (circles and squares) vs y at $m_0/m = 4.0$. The second solvation cumulant is split into the orientational and density components by simulations in the density strained and orientationally relaxed state "NE" (squares) and by freezing solvent translations (circles) in the equilibrium state "E" (Figure 7).

The fact that solutes with $m_0/m = 4.0$ give rise to virtually linear solvent response provide us with a simple route to the solvation entropy. When the system volume is kept constant, temperature enters the system parameters only through y. Changing temperature is thus equivalent to changing y. Therefore, in the LRA, the solvation entropy is

$$Ts_V = -T(\partial\mu_p/\partial T)_V = (y/2)(\partial\langle u_{0s}\rangle/\partial y)_\rho \qquad (28)$$

Similarly to the case of solvation energy, we can consider the orientational and density components of the solvation entropy

$$Ts_V^{or} = (y/2)(\partial\langle u_{0s}\rangle_{NE}^{or}/\partial y)_\rho$$

$$Ts_V^{dens} = (y/2)(\partial\langle u_{0s}\rangle_{NE}^{dens}/\partial y)_\rho \qquad (29)$$

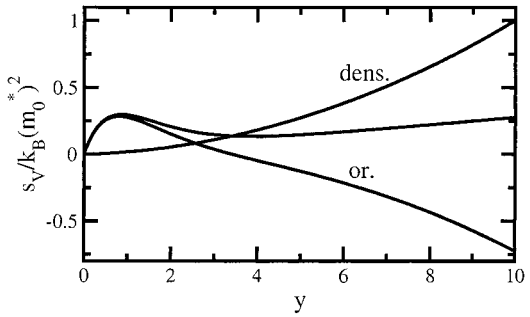

Figure 9. The total constant-volume solvation entropy and its splitting into orientational (or.) and density (dens.) components vs y at $m_0/m = 4.0$.

Figure 9 shows the dependence of the orientational and density components of the solvation entropy on y. Except for a small range of low polarities, the total solvation entropy is mostly independent of y as a result of a compensation between its positive density and negative orientational components. The density component is larger in the absolute magnitude than the orientational component and the total solvation entropy is positive. This result was obtained previously in an analytical model of nuclear reorganization.[37]

The presence of nonlinear solvation makes the LRA connection between the average interaction energy and the solvation chemical potential (eq 7) inapplicable. In the next section, we show how the solvation chemical potential can be obtained in the framework of the Q-model of ET reactions.[41]

4. Thermodynamics of Charge-Transfer Transitions

Equilibrium solvation thermodynamics discussed here has a direct bearing on the thermodynamics of charge-transfer transitions in liquid solvents commonly measured by optical spectroscopy and electron transfer (ET) kinetics. In the course of a vertical Franck−Condon (FC) transition, the solvent electronic polarization changes adiabatically with the changing solute's charge distribution, whereas the nuclear solvent subsystem stays equilibrated with the initial solute's charge distribution. For a charge-separation transition from a nonpolar to polar state, $0 \rightarrow m_0$, the absorption shift is due to electronic solvation only

$$h\Delta\nu_1 = \Delta\mu_{el} \tag{30}$$

where μ_{el} is the solvation chemical potential corresponding to the solvent electronic subsystem. The emission shift includes both the electronic component and the average interaction energy of a dipole with the solvent's nuclear degrees of freedom

$$h\Delta\nu_2 = \langle u_{0s}\rangle + \Delta\mu_{el} \tag{31}$$

where 1 and 2 stand for absorption and emission transitions, respectively.

The two-parameter Marcus−Hush (MH) model of ET[42] employs eqs 7 and 8 to split the vertical average transition *energy* into two equilibrium *free energies*: the equilibrium energy gap and the solvent reorganization energy. For emission transition, one has

$$h\Delta\nu_2 = \Delta\mu_{el} + \frac{1}{2}\langle u_{0s}\rangle - \beta\langle(\delta u_{0s})^2\rangle/2$$

$$= -\lambda_s + \Delta\mu_s \tag{32}$$

where $\Delta\mu_s = \Delta\mu_{el} + \mu_p$ is the solvent component of the equilibrium energy gap and the first term $\lambda_s = (\beta/2)\langle(\delta u_{0s})^2\rangle$ is the solvent reorganization energy. Analogously, for the absorption transition, one has

$$h\Delta\nu_1 = \Delta\mu_{el} + \frac{1}{2}\langle u_{0s}\rangle + \beta\langle(\delta u_{0s})^2\rangle/2$$

$$= \lambda_s + \Delta\mu_s \tag{33}$$

The above splitting (eqs 32 and 33) does not apply when the LRA breaks down indicating that the equilibrium free energy gap, the solvent reorganization energy, and the average vertical transition energy are three independent thermodynamic parameters. One faces then the necessity to replace the two-parameter MH model with a three-parameter alternative.

The three-parameter Q-model was designed to handle problems with nonlinear solvation and those where more flexibility in the parameter space is needed.[41] The theory employs three observables, the Stokes shift and two spectral widths, $h^2\langle(\delta\nu)^2\rangle_2 = \langle(\delta u_{0s}^2)^2\rangle$ and $h^2\langle(\delta\nu)^2\rangle_1 = \langle(\delta u_{0s}^2)^2\rangle_0$, to generate the free energy surfaces of ET and FC factors of optical transitions. For our current discussion of the dipole solvation energetics, the model provides a route to derive the solvation chemical potential from these energy cumulants. For the $0 \rightarrow m_0$ transition, the Stokes shift is identical to $-\langle u_{0s}\rangle$ and one can directly derive the expression for the solvation chemical potential

$$\mu_p = \frac{\langle u_{0s}\rangle}{2} + \frac{\beta\langle(\delta u_{0s})^2\rangle_0\Delta\langle(\delta u_{0s})^2\rangle}{4}\frac{\langle(\delta u_{0s})^2\rangle - 2k_BT\langle u_{0s}\rangle}{[\langle(\delta u_{0s})^2\rangle_0 - 2k_BT\langle u_{0s}\rangle]^2} \tag{34}$$

where $\Delta\langle(\delta u_{0s})^2\rangle = \langle(\delta u_{0s})^2\rangle - \langle(\delta u_{0s})^2\rangle_0$.

The Q-model can be applied if the condition $\gamma = 1$ is fulfilled for the parameter

$$\gamma = \frac{\langle(\delta u_{0s})^2\rangle_0}{\langle(\delta u_{0s})^2\rangle}\left(\frac{\langle(\delta u_{0s})^2\rangle - 2k_BT\langle u_{0s}\rangle}{\langle(\delta u_{0s})^2\rangle_0 - 2k_BT\langle u_{0s}\rangle}\right)^3 \tag{35}$$

The parameter γ calculated from the first and second cumulants over the solute−solvent interaction potential are listed in Table 1. The condition $\gamma = 1$ is fulfilled very well indeed. Consequently, eq 34 can be used to determine the solvation chemical potential. The values of μ_p calculated from eq 35 turn out to be very close to the empirical relation

$$\mu_p = \langle u_{0s}\rangle\frac{\sqrt{\langle(\delta u_{0s})^2\rangle}}{\sqrt{\langle(\delta u_{0s})^2\rangle} + \sqrt{\langle(\delta u_{0s})^2\rangle_0}} \tag{36}$$

(see Figure 10 and Table 1).

Figure 10 shows that the function $-\mu_p(y)$ levels off at $m^* \gg m_0^*$, in qualitative agreement with the prediction of the Onsager model. It may seem that the origin of saturation is irrelevant as long as this limit is actually reached. Note, however, that the fact that the saturation limit is the result of nonlinear solvation simply implies that its outcome depends on the relative magnitudes of the solute, m_0^*, and solvent, m^*, reduced dipoles (from Figure 2, nonlinear solvation starts from about $(m_0^*/m^*)^2 \simeq 2$). The possibility of an experimental verification of solvation saturation thus strongly depends on the magnitudes of solvent and solute dipoles involved in dipolar solvation. Additionally, nonlinear solvation affects the average energy and second solvation cumulant in different ways. This issue is relevant to the problem of calculating the solvent-induced optical band shapes in condensed phases.

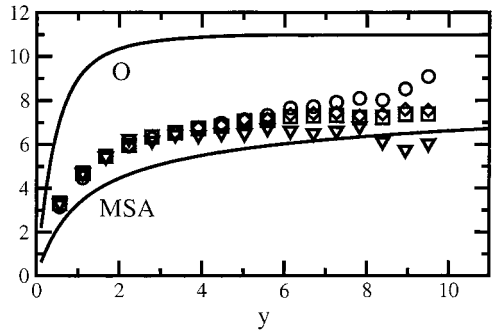

Figure 10. Chemical potential of solvation $-\beta\mu_p$ in the Onsager model (eqs 1 and 2, "O"), in the mean-spherical approximation (MSA),[19] and in the Q-model[41] (eq 34, diamonds; eq 36, squares) at $(m_0^*)^2 = 2.74$. The circles indicate $\beta^2\langle(\delta u_{0s})^2\rangle/2$, down triangles indicate $\beta^2\langle(\delta u_{0s})^2\rangle_0/2$.

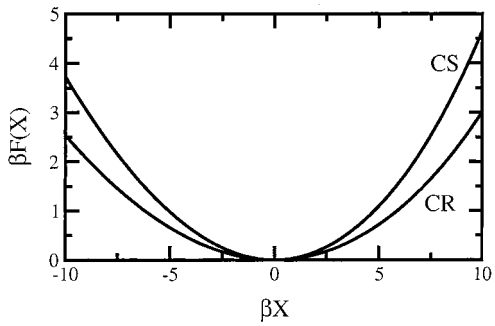

Figure 11. ET free energy surfaces for charge separation (CS, $0 \rightarrow m_0$) and charge recombination (CR, $m_0 \rightarrow 0$) transitions vs the energy gap reaction coordinate X. To facilitate the comparison, the vertexes of two parabolas are shifted to the coordinate origin.

The observation that $\gamma = 1$ holds very accurately for dipole solvation allows one to use the Q-model to build the ET free energy surfaces for charge-separation (CS), $F_1(X)$, and charge-recombination (CR), $F_2(X)$, transitions. The Q-model gives a very simple relation for the ET free energies vs the energy gap reaction coordinate X[41] (for the $0 \rightarrow m_0$ transition, $X = u_{0s}$). The free energy $\Delta F_i(X) = F_i(X) - F_{0i}$ relative to the equilibrium free energy at the surface minimum, F_{0i}, has the following form

$$\Delta F_i(X) = (\sqrt{|\alpha_i||X + \alpha_i\lambda_i - \langle X\rangle_i|} - |\alpha_i|\sqrt{\lambda_i})^2 \quad (37)$$

where $\langle X\rangle_1 = 0$, $\langle X\rangle_2 = \langle u_{0s}\rangle$,

$$\alpha_1 = -\Delta\lambda^{-1}(\lambda_2 - \langle u_{0s}\rangle), \quad \alpha_2 = \alpha_1 + 1 \quad (38)$$

and $\Delta\lambda = \lambda_2 - \lambda_1$. Here, two reorganization energies λ_i are defined through the second cumulants for the neutral and charge-separated states

$$\lambda_1 = \beta\langle(\delta u_{0s})^2\rangle_0/2 \quad \text{and} \quad \lambda_2 = \beta\langle(\delta u_{0s})^2\rangle/2 \quad (39)$$

Figure 11 shows the CS and CR free energy curves calculated according to eq 37 for $(m^*)^2 = 8.5$. As is easy to see, nonlinear solvation effects bring about nonparabolic asymmetry to both the CS and CR curves.

5. Discussion

In the present study, we address the question of whether the saturation limit, predicted by the Onsager model (eq 3), can be observed in model systems. The motivation of the study comes from the contradiction between the Onsager model and molecular, liquid-state solvation theories which do not predict saturation and, instead, yield a linear trend with the dipolar density $\propto y$ at $y \gg 1$, provided the LRA holds. The results of this study can be summarized as follows: (1) A saturation limit for dipole solvation does exist for solid dipolar solvents and does not exist for liquid dipolar solvents within the LRA. (2) Saturation of the liquid solvent response arises from nonlinear solvation when the reduced solute dipole moment m_0^* becomes lower than the reduced solvent dipole m^*. The strongest nonlinear solvation effects are seen for solutes with zero dipole moment. (3) Nonlinear solvation observed at large solvent polarities in liquid solvents is completely due to electrostriction. Nonlinearity is a result of dewetting of solute's surface at $m_0^* < m^*$. (4) The average solvation energy and solvation second cumulant are almost equally affected by orientational and density reorganization in highly polar solvents. (5) The LRA is not applicable in strongly polar solvents and the Q-model of solvation provides a convenient analytical tool allowing to account for nonlinear solvation effects in solvation, optical spectroscopy, and ET reactions.

It is of course reasonable to ask whether the range of y values explored in this study is common for polar solvents employed in solution chemistry. At first glance, the magnitudes of y for which nonlinear solvation takes place are too high. For instance, with the gas-phase dipole moments $m = 1.83$ D and $m = 3.9$ D, one obtains for water and acetonitrile (at normal conditions) $y = 3.8$ and $y = 5.8$, respectively. This estimate neglects, however, the effect of polarizability of the solvent molecular dipoles. Self-consistent models of the thermodynamics of polar−polarizable liquids[13,43] show that the results obtained for nonpolarizable liquids can be applied to polarizable liquids upon the renormalization of the dipolar density $y \rightarrow y'$ with

$$y' = (4\pi/9)\beta\rho(m')^2 + (4\pi/3)\alpha\rho \quad (40)$$

where α is the solvent dipolar polarizability and m' is the condensed-phase dipole moment of the solvent molecules renormalized from its vacuum value m by a self-consistent field of the electronic polarization of the solvent. For water, m' is known to be equal to 2.4 D,[9b] which leads to $y = 6.5$. For acetonitrile, the application of the Wertheim self-consistent approach[43] results in $y = 10.7$.[44] Therefore, it is the necessity to calculate chemical potentials $\mu_p(y')$ that drives our desire to expand the theory to $y' \leq 10$.

The analysis of nonlinear solvation necessitates understanding of the relative importance of dielectric saturation and electrostriction in the solvent response. We found that the effect of dielectric saturation reaches its maximum at intermediate solvent polarities when it is fully compensated by electrostriction of the first solvation shell. The solvent response is linear in that polarity range. Nonlinear effects gain importance at higher polarities and they are fully caused by electrostriction. Contrary to common expectations, the strongest nonlinear solvation effects are seen not for solutes with large dipole moments, but for a solute with zero dipole moment. The major origin of nonlinear solvation is the dewetting of the surface of a nonpolar solute in highly polar solvents when solvent−solvent attractions are not compensated by the solute−solvent forces. Since solvent−solvent interactions present a collective effect, polar states common for optical chromophores can hardly create solute−solvent forces strong enough to compete with solvent−solvent interactions in highly polar solvents. Solvation of nondipolar or weakly dipolar chromophore states may therefore be the main origin of nonlinear solvation effects in optical experiments.

The Onsager model for dipole solvation is widely used in optical spectroscopy to correlate solvent-induced spectral shifts

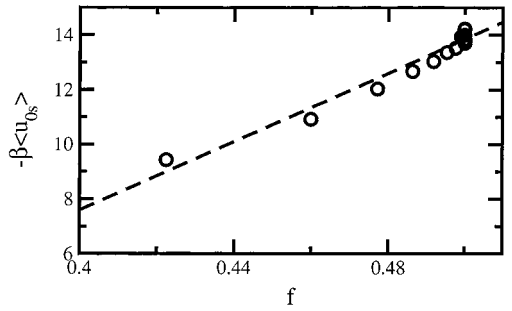

Figure 12. Lippert−Mataga plot of the Stokes shift ($-\beta\langle u_{0s}\rangle$) obtained from simulations (points) vs the dielectric parameter f (eq 41). The dashed line is a linear regression through the points.

with solvent dielectric properties.[2,3] In particular, the solvent dependence of the Stokes shift is often described with the parameter

$$f = \frac{\epsilon - 1}{2\epsilon + 1} - \frac{\epsilon_\infty - 1}{2\epsilon_\infty + 1} \tag{41}$$

where ϵ_∞ is the high-frequency dielectric constant; $\epsilon_\infty = 1$ in our model. The existence of a linear trend of the Stokes shift (equal to $-\langle u_{0s}\rangle$ in our model) with f calculated in different solvents often serves to validate the continuum model and/or the LRA. Figure 12 shows the same dependence, known as Lippert−Mataga plot,[3] with our simulation data and f calculated according to eqs 5 and 41 for $(m^*)^2 \geq 1.0$. Except for the most polar solvents, which can be easily missed in a limited range of solvents experimentally available, there is a linear trend of $-\beta\langle u_{0s}\rangle$ vs f. [In real solvents, molecular quadrupoles make the dependence $\epsilon(y)$ less sharp[13] resulting in an even better linear trend on the Lippert−Mataga plot]. This analysis indicates that the existence of the Lippert−Mataga dependence validates neither continuum model nor the LRA. The solvent polarity parameter $f(\epsilon)$ is merely a good probe function going from zero at low polarities to a saturation limit at high polarities. For liquid solvents, however, this saturation occurs only due to local density changes of the solvent around the solute not included in continuum models. Furthermore, these local density changes give rise to nonlinear solvation that is responsible for saturation. No saturation exists within the LRA.

The entropy of solvation at constant volume was calculated from the polarity dependence of the average solvation energy when the LRA holds ($m_0/m = constant$). The entropy was also separated into the contributions arising from orientational and density solvent reorganization. The two components turned out to have opposite signs, with the total positive solvation entropy originating from the higher magnitude of its positive density component. Nuclear solvent reorganization considered here is responsible for the Stokes shift in optical experiments and for the solvent reorganization energy in ET reactions. These parameters are often calculated using the Onsager model[2−5] which, as well as other dielectric cavity models, includes only the orientational reorganization.[37] For dipolar solvation, the orientational solvation entropy can be estimated from the temperature derivative of the polarity parameter f in eq 41. To avoid the uncertainty in choosing the cavity radius, we consider the ratio $-s_V T/\mu_p$, which is given in the Onsager model by the relation

$$-\frac{s_V T}{\mu_p} = \frac{3T}{f}\left[\frac{1}{(2\epsilon+1)^2}\left(\frac{\partial\epsilon}{\partial T}\right)_V - \frac{1}{(2\epsilon_\infty+1)^2}\left(\frac{\partial\epsilon_\infty}{\partial T}\right)_V\right] \tag{42}$$

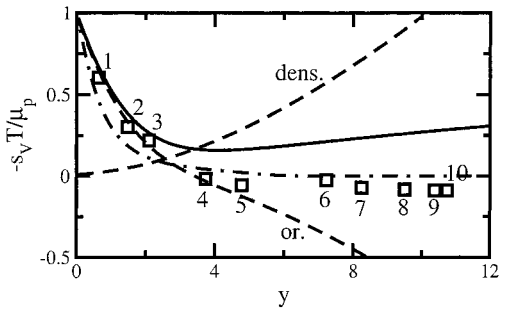

Figure 13. The ratio of the entropy of dipole solvation to the solvation chemical potential vs y in the Onsager model (dash−dotted line) and from MC simulations ($m_0/m = 4.0$): $-2s_V T/\langle u_{0s}\rangle$ (solid line), $-2s_V^{or} T/\langle u_{0s}\rangle$ (or), and $-2s_V^{dens} T/\langle u_{0s}\rangle$ (dens). Points refer to the ratios given by eq 42 vs y', where y' was calculated by a combined application of the Kirkwood and Kirkwood−Fröhlich equations according to ref 44b. The numbers on the plot indicate chloroform (1), tetrahydrofuran (2), 1,1-dichloroethane (3), acetone (4), propionitrile (5), dimethylformamide (6), nitromethane (7), acetonitrile (8), dimethyl sulfoxide (9), and propylene carbonate (10).

This ratio, estimated for 10 commonly used solvents,[45] is shown in Figure 13 (points, solvent parameters from refs 35 and 46) and compared to the corresponding ratio from the present simulations (solid line) and from the Onsager model for dipolar HSs (dash−dotted line, eqs 1, 2, and 5). The results of calculations according to eq 42 fall very close to the prediction of the Onsager model for dipolar HSs, but yield slightly negative entropies at large y. On the contrary, the simulations yield positive and much higher in the absolute value ratios $-s_V T/\mu_p$, pointing to a more substantial entropic component in the solvation chemical potential than that given by the Onsager model. The latter, applied to both model and real solvents, is unable to give even a qualitative account of solvation entropies in highly polar solvents. Positive entropies of nuclear reorganization were predicted previously in the framework of an analytical model[37] and subsequently confirmed by experiment.[44b,47]

There is a fairly good agreement between solvation entropies from eq 42 and the orientational entropy from our simulations at $y \leq 5$ (Figure 13). At larger y values, the solvation entropy from eq 42 levels off at a slightly negative magnitude, whereas the simulated orientational entropy continues to decay. It is not yet clear whether the Onsager model gives a correct estimate of the orientational entropy and if one can apply the results obtained here for HS dipolar liquid solvents to highly polar molecular solvents. Molecular polarizability and higher multipoles of the solvent molecules should be included for a more realistic analysis, which will be a subject of future research.

The present study is based on the cumulant route to the solvation chemical potential.[48−50] Only two first cumulant are measured by computer simulations and the Q-model of nonlinear solvation[41] is used to generate μ_p. The Q-model is based on an infinite-cumulant expansion to construct the free energy surfaces of solvation as functions of the soolute-solvent interaction potential. The model consistency in application to many-body problems requires that the parameter γ, given by eq 35, is equal to unity. This condition is fulfilled very accurately for our present simulations (Table 1). This allows us to use the full potential of the Q-model to calculate not only the solvation chemical potential (eq 34), but also the free energies of ET reactions and FC factors of optical transitions. As is shown in Figure 7, solvation nonlinearities manifest themselves in a significant difference between the CS and CR free energy surfaces,[51] as well as in the asymmetry of each individual ET free energy surface.[52]

A truncated cumulant expansion in the solute−solvent interaction potential is used in approximate calculations of the solvation chemical potential from a few first cumulants available from computer simulations.[48−50] An expansion around several states with different degree of the solute−solvent coupling improves the interpolation accuracy,[48,49a] and when a sufficient number of intermediate states is available, the thermodynamic integration technique[9a] yields the solvation chemical potential. There are other simulation protocols directly leading to free energies (for a review see ref 53). Among those, expanded ansemble simulations[54] and hystogram reweighting[55,56] are effective alternatives to the cumulant expansion and thermodynamic integration.

Given poor convergence and potential system-size dependence of higher-order expansion terms, simulations are often limited to only two first cumulants[49b,c,50] (four cumulants are reported by Hummer et al.[49a] for the problem of water hydration). The second-order truncated cumulant expansion leads to the following interpolation relation for the solvation chemical potential[48]

$$\mu_p = \frac{\langle u_{0s}\rangle}{2} + \frac{\beta\Delta\langle(\delta u_{0s})^2\rangle}{12} \qquad (43)$$

Equation 43 can be obtained also from eq 34 of the Q-model if one assumes $\langle(\delta u_{0s})^2\rangle_0 = \langle(\delta u_{0s})^2\rangle = -2k_BT\langle u_{0s}\rangle$ in the last term in eq 34 while still keeping $\Delta\langle(\delta u_{0s})^2\rangle \neq 0$. The advantage of the Q-model over truncated cumulant expansions is that it based on an infinite series of cumulants. However, it does not specify how well the consistency condition $\gamma = 1$ should be obeyed for an accurate estimate of μ_p. An insight into such a criterion can be gained from the simulation results by Hummer and Szabo.[48b] For the process of charging a water molecule in the bulk water solvent, they report $-\beta\langle u_{0s}\rangle = 39.62$, $\beta^2\langle(\delta u_{0s})^2\rangle = 71.66$, and $\beta^2\langle(\delta u_{0s})^2\rangle_0 = 17.99$. With these parameters, $\gamma = 0.938$ and the Q-model gives $-\beta\mu_p = 15.95$, about 11% higher than the value of 14.40 following from the thermodynamic integration.[9a,49a] This example allows us to suggest that $\gamma = 1.00 \pm 0.05$ is required for a reliable estimate of the chemical potential of solvation from the Q-model. Direct simulations of the solvation chemical potential are necessary for further tests of the Q-model and a better understanding of the polarity dependence of multipole solvation in polar solvents.

Acknowledgments are made to the donors of the Petroleum Research Fund, administered by the ACS (36404-G6), and to the start-up fund by the Department of Chemistry and Biochemistry at ASU, for support of this research.

References and Notes

(1) Onsager, L. *J. Am. Chem. Soc.* **1936**, *58*, 1486.

(2) (a) Liptay, W. In *Modern Quantum Chemistry, Part II*; Sinanoğlu, O., Ed.; Academic Press: New York, 1965. (b) Suppan, P. J. *Photochem. Phobiol.* **1990**, *50*, 293.

(3) Mataga, N. *Molecular Interactions and Electronic Spectra*; Marcel Dekker: New York, 1970.

(4) (a) Maroncelli, M.; Fleming, G. R. *J. Chem. Phys.* **1987**, *86*, 6221. (b) Loring, R. F.; Yan, Y. J.; Mukamel, S. *J. Chem. Phys.* **1987**, *87*, 5840. (c) Hsu, C.-P.; Georgievskii, Y.; Marcus, R. A. *J. Chem. Phys. A* **1998**, *102*, 2658.

(5) (a) Nee, T. W.; Zwanzig, R. *J. Chem. Phys.* **1970**, *52*, 6353. (b) Hubbard, J. B.; Wolynes, P. G. *J. Chem. Phys.* **1978**, *63*, 998. (c) Maroncelli, M. *J. Chem. Phys.* **1997**, *106*, 1545.

(6) Abe, T. *J. Phys. Chem.* **1986**, *90*, 713.

(7) Ehrenson, S. *J. Phys. Chem.* **1987**, *91*, 1868.

(8) Basilevsky, M. V.; Parsons, D. F. *J. Chem. Phys.* **1996**, *105*, 3734.

(9) (a) Rick, S. W.; Berne, B. J. *J. Am. Chem. Soc.* **1994**, *116*, 3949. (b) Bader, J. S.; Berne, B. J. *J. Chem. Phys.* **1996**, *104*, 1293. (c) Bader, J. S.; Cortis, C. M.; Berne, B. J. *J. Chem. Phys.* **1997**, *106*, 2372.

(10) (a) Blum, L.; Fawcett, W. R. *J. Phys. Chem.* **1996**, *100*, 10423. (b) Fawcett, W. R. *J. Phys. Chem. B* **1999**, *103*, 11181.

(11) Roux, B.; Yu, H.-A.; Karplus, M. *J. Phys. Chem.* **1990**, *94*, 4683.

(12) Cramer, C. J.; Truhlar, D. G. *Chem. Rev.* **1999**, *99*, 2161.

(13) Stell, G.; Patey, G. N.; Høye, J. S. *Adv. Chem. Phys.* **1981**, *18*, 185.

(14) Gray, C. G.; Gubbins, K. E. *Theory of Molecular Fluids. Volume 1: Fundamentals*; Clarendon Press: Oxford, 1984.

(15) Böttcher, C. J. F. *Theory of Electric Polarization*; Elsevier: Amsterdam, 1973.

(16) (a) Warshel, A. *Computer Modeling of Chemical Reactions in Enzymes and Solutions*; Wiley: New York, 1991. (b) Papazyan, A.; Warshel, A. *J. Chem. Phys.* **1997**, *107*, 7975. (b) Florián, J.; Warshel, A. *J. Phys. Chem. B* **1999**, *103*, 10282.

(17) Tani, A.; Henderson, D.; Barker, J. A.; Hecht, C. E. *Mol. Phys.* **1983**, *48*, 863.

(18) Matyushov, D. V.; Ladanyi, B. M. *J. Chem. Phys.* **1999**, *110*, 994.

(19) Isbister, D.; Bearman, R. *J. Mol. Phys.* **1974**, *28*, 1297.

(20) Matyushov, D. V.; Ladanyi, B. M. *J. Chem. Phys.* **1997**, *107*, 1362.

(21) Madden, P.; Kivelson, D. *Adv. Chem. Phys.* **1984**, *56*, 467.

(22) Abramowitz, M.; Stegun, I. A. *Handbook of Mathematical Functions*; Dover Publications, Inc.: New York, 1972.

(23) Stanley, H. E. *Introduction to Phase Transitions and Critical Phenomena*; Oxford University Press: New York, 1971.

(24) Neumann, M. *Mol. Phys.* **1986**, *57*, 97.

(25) Wertheim, M. S. *J. Chem. Phys.* **1971**, *55*, 4291.

(26) (a) Fries, P. H.; Patey, G. N. *J. Chem. Phys.* **1985**, *82*, 429. (b) Wei, D.; Patey, G. N.; Perera, A. *Phys. Rev. E* **1993**, *47*, 506.

(27) The slope of $\langle(\delta u_{0s})^2\rangle$ vs y at $y \gg 1$ with $m_0/m = 4.0$ (simulations) is reproduced by eq 19 with $\kappa_T \simeq 0.9$.

(28) We use here a broader than usual understanding of electrostriction defining it as a density change in an external electric field. The dewetting effects observed here are then classified as electrostriction as well.

(29) Jayaram, B.; Fine, R.; Sharp, R.; Honig, B. *J. Phys. Chem.* **1989**, *93*, 4320.

(30) Åqvist, J.; Hansson, T. *J. Phys. Chem.* **1996**, *100*, 9512.

(31) Åqvist and Hansson[30] did not observe any electrostriction in their simulations. In this sense, the present simulations of solvation in polar lattices mimic the situation that may exist in strongly associated liquid solvents.

(32) Stillinger, F. H. *J. Solut. Chem.* **1973**, *2*, 141.

(33) Hummer, G.; Garde, S. *Phys. Rev. Lett.* **1998**, *80*, 4193.

(34) Tang, Z.; Scriven, L. E.; Davis, H. T. *J. Chem. Phys.* **1992**, *96*, 4639.

(35) Schmid, R.; Matyushov, D. V. *J. Phys. Chem.* **1995**, *99*, 2393.

(36) (a) Bagchi, B.; Chandra, A. *Adv. Chem. Phys.* **1991**, *80*, 1. (b) Biswas, R.; Bagchi, B. *J. Phys. Chem.* **1996**, *100*, 4261.

(37) Matyushov, D. V. *Chem. Phys.* **1993**, *174*, 199.

(38) Barbara, P. F.; Jarzeba, W. *Adv. Photochem.* **1990**, *15*, 1.

(39) (a) Stratt, R. M.; Cho, M. *J. Chem. Phys.* **1994**, *100*, 6700. (b) Ladanyi, B. M.; Stratt, R. M. *J. Phys. Chem.* **1995**, *99*, 2502.

(40) (a) Ladanyi, B. M.; Maroncelli, M. *J. Chem. Phys.* **1998**, *109*, 3204. (b) Steele, W. A. *Mol. Phys.* **1987**, *61*, 1031.

(41) Matyushov, D. V.; Voth, G. A. *J. Chem. Phys.* **2000**, *113*, 5413.

(42) Marcus, R. A. *Rev. Mod. Phys.* **1993**, *65*, 599.

(43) (a) Wertheim, M. S. *Mol. Phys.* **1979**, *37*, 83. (b) Venkatasubramanian, V.; Gubbins, K. E.; Gray, C. G.; Joslin, C. G. *Mol. Phys.* **1984**, *52*, 1411. (c) Joslin, C. G.; Gray, C. G.; Gubbins, K. E. *Mol. Phys.* **1985**, *54*, 1117.

(44) (a) Matyushov, D. V. *Chem. Phys.* **1996**, *211*, 47. (b) Vath, P.; Zimmt, M. B.; Matyushov, D. V.; Voth, G. A. *J. Phys. Chem. B* **1999**, *103*, 9130.

(45) Experimental derivatives of dielectric constants over temperature are available only at constant pressure.[46] These were used instead of derivatives at constant volume in eq 42.

(46) (a) Riddick, J. A.; Bunger, W. B.; Sakano, T. K. *Organic Solvents, V. II*; Wiley: New York, 1986. (b) Marcus, Y. *Ion Solvation*; Wiley: New York, 1986.

(47) (a) Nelsen, S. F.; Ismagilov, R. F.; Gentile, K. E.; Powell, D. R. *J. Am. Chem. Soc.* **1999**, *121*, 7108. (b) Derr, D. L.; Elliott, C. M. *J. Phys. Chem. A* **1999**, *103*, 7888. (c) Vath, P.; Zimmt, M. B. *J. Phys. Chem. A* **2000**, *104*, 2626.

(48) (a) Zhou, H.-X.; Szabo, A. *J. Chem. Phys.* **1995**, *103*, 3481. (b) Hummer, G.; Szabo, A. *J. Chem. Phys.* **1996**, *105*, 2004.

(49) (a) Hummer, G.; Pratt, L. R.; Garcia, A. E. *J. Phys. Chem.* **1995**, *99*, 14188. (b) Hummer, G.; Pratt, L. R.; Garcia, A. E. *J. Phys. Chem.* **1996**, *100*, 1206. (c) Garde, S.; Hummer, G.; Paulaitis, M. E. *J. Chem. Phys.* **1998**, *108*, 1552.

(50) Morillo, M.; Denk, C.; Sánches-Burgos, F.; Sánchez, A. *J. Chem. Phys.* **2000**, *113*, 2360.

(51) (a) Kakitani, T.; Mataga, N. *J. Phys. Chem.* **1985**, *89*, 8. (b) Kakitani, T.; Mataga, N. *J. Phys. Chem.* **1985**, *89*, 4752.
(52) Tachiya, M. *Chem. Phys. Lett.* **1989**, *159*, 505.
(53) Kofke, D. A.; Cummings, P. T. *Mol. Phys.* **1997**, *92*, 973.
(54) (a) Liu, Z.; Berne, B. J. *J. Chem. Phys.* **1993**, *99*, 6071. (b) Poés, R.; Eisenmesser, E.; Post, C. B.; Roux, B. *J. Chem. Phys.* **1999**, *111*, 3387.
(55) (a) Ferrenberg, A. M.; Swendsen, R. *Phys. Rev. Lett.* **1988**, *61*, 2635. (b) Ferrenberg, A. M.; Swendsen, R. *Phys. Rev. Lett.* **1989**, *63*, 1195. (c) Ferrenberg, A. M.; Landau, D. P.; Swendsen, R. *Phys. Rev. E* **1995**, *51*, 5092.
(56) Kiyohara, K.; Gubbins, K. E.; Panagiotopoulos, A. Z. *J. Chem. Phys.* **1997**, *106*, 3338.